Available online at www.sciencedirect.com

SciVerse ScienceDirect

Ceramics International 39 (2013) 2353–2358

CERAMICS INTERNATIONAL

www.elsevier.com/locate/ceramint

Synthesis, characterization, and thermoelectric properties of nanostructured bulk p-type $MnSi_{1.73}$, $MnSi_{1.75}$, and $MnSi_{1.77}$

Zahra Zamanipour[a,1], Xinghua Shi[a,1], Masoud Mozafari[b], Jerzy S. Krasinski[a], Lobat Tayebi[b,c], Daryoosh Vashaee[a,*]

[a]Helmerich Advanced Technology Research Center, School of Electrical and Computer Engineering, Oklahoma State University, Tulsa, OK 74106, USA
[b]Helmerich Advanced Technology Research Center, School of Material Science and Engineering, Oklahoma State University, Tulsa, OK 74106, USA
[c]School of Chemical Engineering, Oklahoma State University, Stillwater, OK 74078, USA

Received 11 July 2012; received in revised form 16 July 2012; accepted 28 August 2012
Available online 6 September 2012

Abstract

P-type higher manganese silicide (HMS) has attracted considerable interest due to its remarkable thermoelectric (TE) properties and potential applications at intermediate and high temperature TE devices. In this study, a series of nanostructured bulk p-type HMS materials with different compositions of $MnSi_x$ (where $x=1.73$, 1.75 and 1.77) were synthesized via mechanical ball milling and hot-press sintering. The X-ray diffraction analysis of the synthesized materials showed that increasing the Si contents yields to a slight shift to higher diffraction angles. The increase in Si content further resulted in a decrease in electrical conductivity and increase in Seebeck coefficient. The power factor of all three compositions are approximately identical. However, the lowest thermal conductivity was achieved in $MnSi_{1.75}$ and resulted in the highest figure-of-merit among all the compositions.

Keywords: Higher manganese silicide; Thermoelectric properties; Nanostructured materials

1. Introduction

Recently there have been significant efforts to develop efficient thermoelectric materials for cooling and energy harvesting applications. The performance of a thermoelectric material depends on dimensionless figure-of-merit, ZT, which is defined by

$$ZT = \frac{S^2\sigma}{\kappa}\ T = \frac{P_F T}{\kappa} \quad (1)$$

where S is the Seebeck coefficient, σ is the electrical conductivity, κ is the thermal conductivity, T is the absolute temperature, and P_F is the thermoelectric power factor [1].

There have been significant efforts in generating thermoelectric materials based on $(Bi,Sb)_2(Te,Se)_3$, PbTe, and Si_xGe_{1-x} alloys in the past. While each material system covers certain range of working temperature ($(Bi,Sb)_2(Te,Se)_3$ 0–200 °C, PbTe 300–500 °C, and SiGe 800–1100 °C), there is a gap for the range of medium to high temperature range, namely 400–900 °C.

Nanostructuring has offered a new approach to enhance the efficiency of thermoelectric materials. $(Bi,Sb)_2Te_3$, Si_xGe_{1-x}, and Si bulk nanostructured materials have already shown enhanced ZT [1–4], due to the reduction in thermal conductivity (κ) without significantly affecting the thermoelectric power factor ($S^2\sigma$) [5,6]. On similar concepts, certain materials with higher power factors are expected to make good thermoelectric materials if they can be synthesized into nanostructured form. Since transition metal silicides have shown a good power factor for operating temperature range of 400–800 °C, nanostructuring may help to improve their thermoelectric efficiency. Among them alloys of silicon and manganese with higher Si content such as $Mn_{11}Si_{19}$, $Mn_{15}Si_{26}$, $Mn_{27}Si_{47}$ and Mn_4Si_7 have shown power factor ($S^2\sigma$) approaching $\sim 2\times10^{-3}$ W/m K^2 [1]. Higher manganese silicide (HMS)

*Corresponding author. Tel.: +1 918 594 8017; fax: +1 270 897 1179.
E-mail address: daryoosh.vashaee@okstate.edu (D. Vashaee).
[1]Xinghua Shi and Zahra Zamanipour contributed equally to this work.

0272-8842/$ - see front matter © 2012 Elsevier Ltd and Techna Group S.r.l. All rights reserved.
http://dx.doi.org/10.1016/j.ceramint.2012.08.086

compounds make Chimney-ladder structures with a bandgap around 0.7 eV [1]. These compounds may also contain nano- to micro-scale regions of manganese monosilicide (MnSi) which can reduce the thermal conductivity [7–10].

Large Seebeck coefficient, low resistivity, high oxidation resistance, and non-toxicity [7,11,12] make the HMS alloy a good candidate in thermoelectric device applications especially for mid to high temperature range devices. It is inexpensive and mechanically robust with lower density than Bismuth and Chalcogenide based alloys owing to the small density of Silicon. In comparison, alloys based on PbTe have shown enhanced thermoelectric figure-of-merit at medium temperature [13]. However, both Pb and Te are toxic. The non-toxicity, stability, and low cost of HMS make it a promising TE material especially for large scale energy harvesting applications.

Compound of $MnSi_{1.73}$ has been made via a powder metallurgical route [14] and characterized for its thermoelectric properties. $MnSi_{1.8}$ and $MnSi_{1.85}$ compounds have also been produced via mechanical alloying and pulse discharge sintering [15]. $MnSi_{1.7}$ powder has also been produced via gas atomization, which is appropriate for large scale production [16]. Compared with fabrication methods such as arc melting, induction heating, or conventional crystal growth methods, powder metallurgical methods have advantages for better structural homogeneity and smaller amounts of energy consumption [17].

In this report, we focused on mechanical alloying approach to produce thermoelectric alloys of $MnSi_x$ with different silicon contents ranging from $x=1.73$ to 1.77. The produced powders were sintered via the hot-press method to achieve nanostructured bulk structure. Their structural parameters and thermoelectric properties were characterized and discussed.

2. Materials and methods

2.1. Synthesis of HMS powder

The HMS powder was prepared from 100 mesh silicon and 325 mesh manganese powders from Alfa Aesar Co. with purity of 99.9% and 99.99%, respectively. The amount of each component was weighed in an argon-filled glove box for different compositions of $MnSi_x$ with $x=1.73$, 1.75, and 1.77. The mixed powder with the tungsten carbide balls was loaded into tungsten carbide bowels and milled in planetary mill with ball to powder weight ratio (BPR) of five. Both Fritsch's planetary ball mills P6 (500 rpm) and P7 (1000 rpm) were used. The speeds are equal to centrifugal acceleration of about $22G$ and $86G$, respectively, where G is the gravitational constant. All the powders were dry milled for approximately 50 h. The milled powders were weighted and loaded into a graphite die with inner diameter of 12.7 mm. All three samples were sintered at 950 °C for 5 min under 108 MPa pressure. These milling and synthesis parameters were optimized by making and characterizing over two hundreds of different HMS samples.

2.2. Characterization

The cylindrical samples were cut into rectangular bars and circular discs for electrical resistivity and thermal conductivity measurements, respectively. To determine the thermoelectric properties, the Seebeck coefficient (S) and electrical conductivity (σ) were measured from room temperature to 970 K using a ZEM system (ULVAC Riko Co.) equipped with a four probe contact measurement facility. The thermal conductivities were measured using the laser flash method with Netzsch's LFA 457 Micro Flash equipment.

The samples were structurally evaluated by performing scanning electron microscopy (SEM) using a Hitachi S-4800. X-ray diffraction (XRD) analysis was performed in the range of $20^\circ < 2\theta < 60^\circ$ using Bruker AXS D8 with Cu Kα radiation ($\lambda=1.54056$ Å).

To study the thermal behavior and melting point of the samples, differential thermal analysis (DTA, Netzsch, STA 449 F1 Jupiter®) was accomplished with heating rate of 20 K/min under flowing argon atmosphere in an alumina crucible.

3. Results and discussions

3.1. Structural analysis

The XRD patterns of the $MnSi_{1.75}$ powder milled at 500 rpm with different milling times are shown in Fig. 1. It is shown that some small characteristic peaks of Mn and Si continuously decreased with milling time while the HMS peaks grow. The Mn and Si peaks diminished after approximately 12 h of milling. It can be also seen that MnSi was presented in the samples until 16 milling hours, which decreased and diminished after 80 h of milling. At this point, all the major characteristic peaks of pure HMS appeared and were in good agreement with those reported by Karpinsky and Evseev [18]. When comparing the

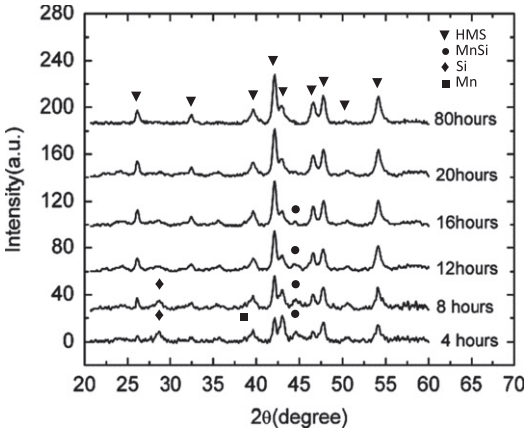

Fig. 1. XRD patterns of HMS powder after different milling times.

diffraction peaks, it is difficult to distinguish the real structure of HMS from the XRD data as the position of the peaks are weak functions of the exact composition of HMS. These observations can explain why the exact structure of HMS is rarely given in the literature. Compared with Zhou et al. who reported HMS composition variation resulted from oxidation of Mn and Si during milling [19], we did not observe any oxidation even in powders milled up to 80 h.

The XRD patterns of the hot pressed samples with three different HMS compositions were collected and shown in Fig. 2. One can observe that the diffraction peak at $2\theta = 53.8^\circ$ is shifted towards higher angles from $MnSi_{1.73}$ (red curve) to $MnSi_{1.77}$ (black curve). Moreover the relative intensities corresponding to this peak is considerably changed with the sample with highest Si content ($MnSi_{1.77}$) having the highest peak intensity. The XRD results indicate that three different composition of HMS were generated in the process.

Fig. 3 shows the SEM micrographs of the fracture surface of sintered $MnSi_{1.75}$ in three different magnifications. As can be seen here, voids of 5–200 μm in size in both intergranular and transgranular fractures were formed in the sample. The size of the primary grains ranged from 200 nm to 800 nm.

Analyzing the DTA thermographs of the three different HMS compositions indicated no significant correlation between the main melting point within the range of our experiment (e.g. $x = 1.73$, 1.75 and 1.77). According to the thermographs of different samples presented in Fig. 4, a slight difference in melting point of different compositions was observed. The melting points are 1146.4, 1147.3 and 1149.0 °C for $MnSi_{1.73}$, $MnSi_{1.73}$ and $MnSi_{1.73}$, respectively. To the best of our knowledge there is no reporting data in this regard which indicates the melting point versus composition. Understanding of the physical reason for the small shift of melting point and the influence of Si on the structural properties needs to be investigated. Recently Borman et al. [20] introduced a theoretical description of melting point for nanostructured materials in the framework of a uniform approach using vacancy mechanism. In this framework the change of melting point with nanostructuring was described as a result of anharmonic oscillations of atoms. All in all, it seems that totally understanding the effect of Si on the structure and melting point of different samples from the bottom up is a daunting challenge.

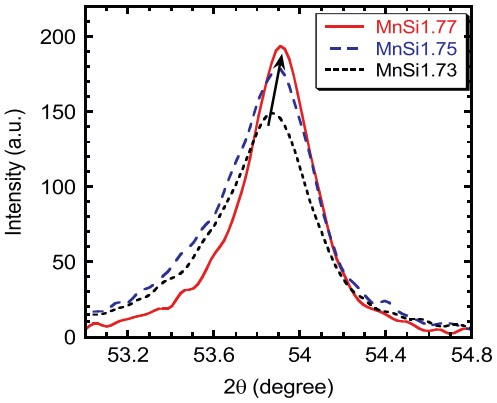

Fig. 2. Diffraction peak at $2\theta = 53.8^\circ$ for different HMS compositions.

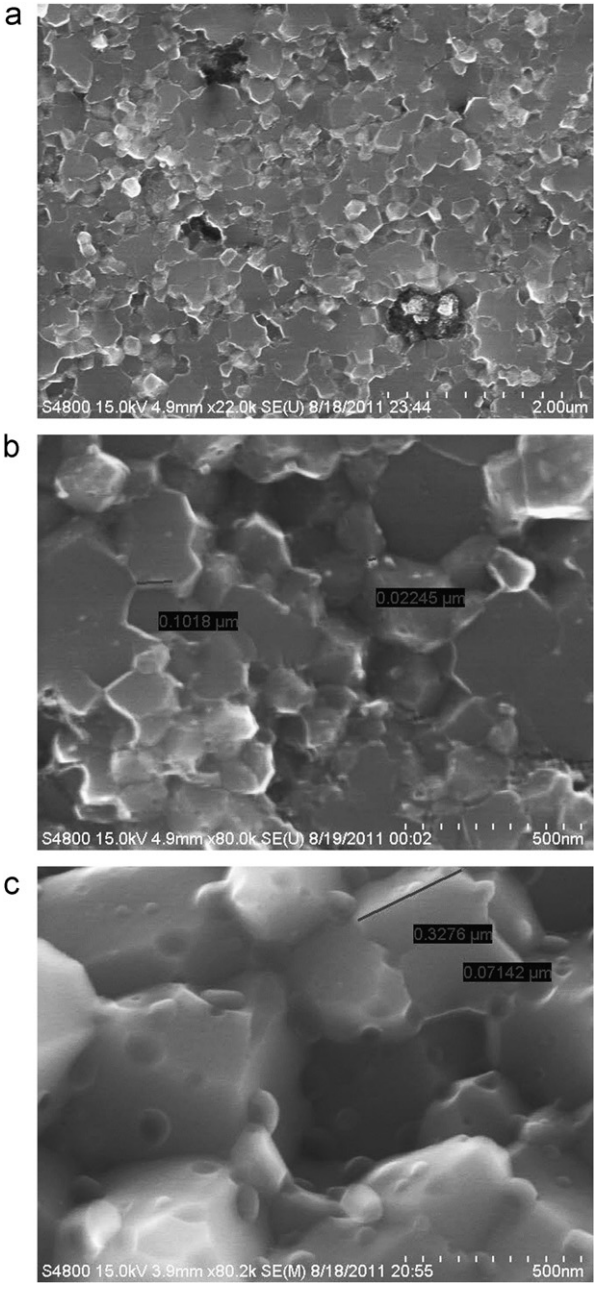

Fig. 3. SEM micrographs of sample $MnSi_{1.75}$ with different magnifications: (a) ×22.0 k (b) ×80.0 k and (c) ×80.2 k.

3.2. Effect of composition on thermoelectric properties

Fig. 5 shows the temperature dependence of electrical conductivity for all three sintered $MnSi_{1.73}$, $MnSi_{1.75}$, and $MnSi_{1.77}$ samples. As shown in this figure, the electrical conductivity decreases with temperature.

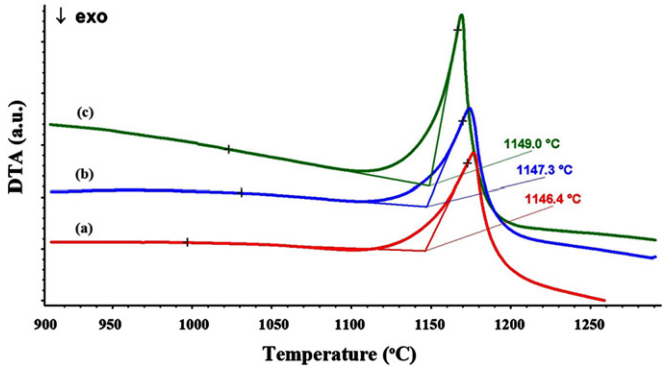

Fig. 4. DTA thermographs of different $MnSi_x$ samples in the range of 900–1300 °C. (a) $MnSi_{1.73}$, (b) $MnSi_{1.75}$, and (c) $MnSi_{1.77}$.

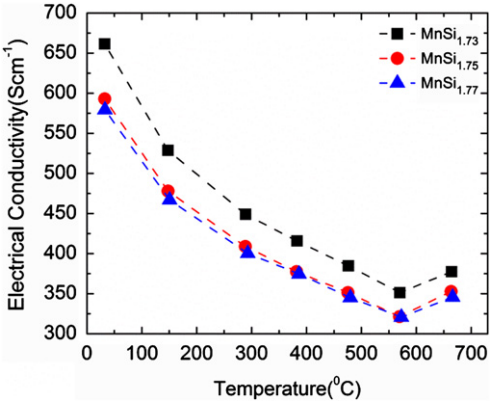

Fig. 5. Electrical conductivity of different $MnSi_x$ samples versus temperature.

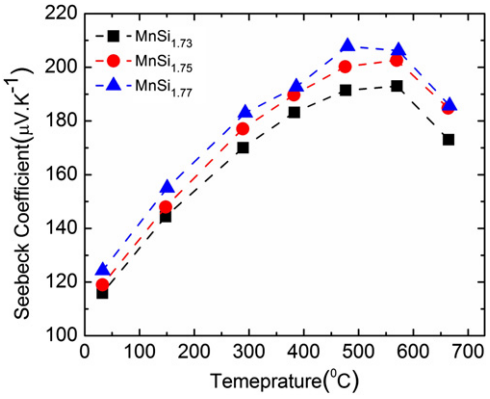

Fig. 6. Seebeck coefficient trend of different $MnSi_x$ samples versus temperature.

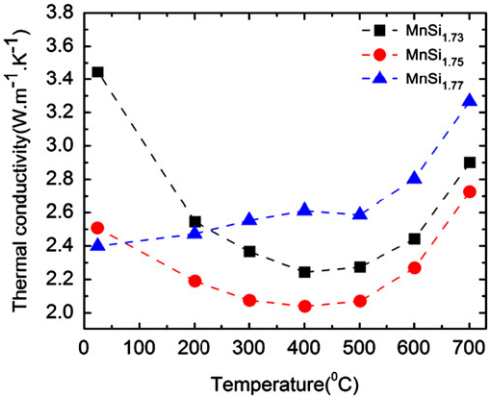

Fig. 7. Thermal conductivity of different $MnSi_x$ samples versus temperature.

Since the electron-acoustic phonon scattering rate increases with temperature, the charge carrier mobility decreases and consequently the electrical conductivity decreases. This decrease happens up to about 580 °C at which point by further increase of the temperature electrons, which are the minority carriers, are thermally excited and involve in transport phenomena yielding a small increase in electrical conductivity. Although this trend is same in all semiconductors, the turning point depends on the band gap of the material. Similar trend for electrical conductivity are reported [21–23]. Here, the electrical conductivity of $MnSi_{1.73}$ sample was slightly higher than $MnSi_{1.75}$ and $MnSi_{1.7}$ samples.

It is known that the charge carrier concentration and the grain boundary scattering both determine the Seebeck coefficient trends [3]. Seebeck coefficient versus temperature is shown in Fig. 6 for all three samples. Seebeck coefficient in all samples increases up to 580 °C and then decreases at higher temperatures. It is seen that Seebeck coefficient trend is reversed compared with the temperature dependence of electrical conductivity (Fig. 5).

Fig. 7 shows the thermal conductivity of all three structures as a function of temperature. The thermal conductivity of the samples decreased with temperature up to about 500 °C. The initial reduction in thermal conductivity is due to the increase of phonon–phonon scattering which reduced the lattice part of thermal conductivity. However, the thermal conductivity increases rapidly as temperature increases above 500 °C. This is due to the enhancement of ambipolar thermal conduction. Ambipolar thermal conduction is a result of thermal excitation of electrons. Similar trend is reported in previous works [24]. HMS is known to have an indirect band gap of 0.77 eV [25], which is small compared with high temperature thermoelectric materials such as $Si_{0.8}Ge_{0.2}$. The thermal excitation of minority carriers enhances significantly at around 500 °C, which limits further increase of Seebeck coefficient and reduction of thermal conductivity. As a result the ZT has a turning point at around 500 °C with a decreasing trend at higher temperature as shown in Fig. 9.

It is worth mentioning that the increment of silicon amount in HMS structure increased the electrical conductivity and decreased Seebeck coefficient. The power factor times temperature (PFT) versus temperature for all compositions are shown in Fig. 8. It can be seen that the power factor time temperature is approximately identical for all three different compositions with maximum value of 1.15 W/mK at 600 °C. The figure-of-merit, ZT, of all

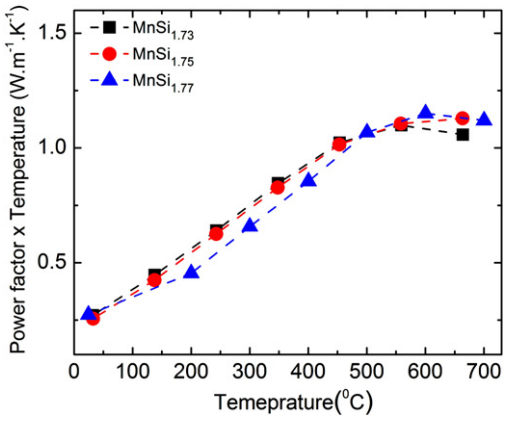

Fig. 8. Power factor of different $MnSi_x$ samples versus temperature.

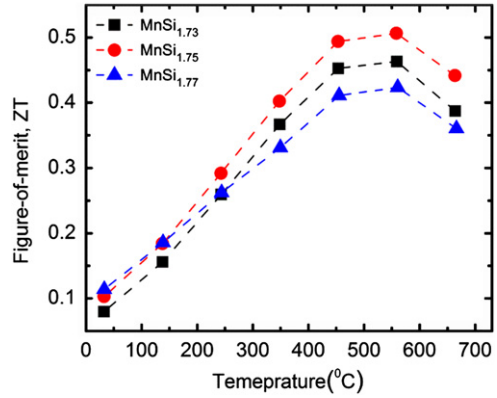

Fig. 9. ZT of different $MnSi_x$ samples versus temperature.

sintered samples are shown in Fig. 9. The ZT for all samples has a maximum around 600 °C after which it decreases. According to the ZT data versus temperature, it can be concluded that all three compositions have the optimum operation temperature range of 450–650 °C. $MnSi_{1.77}$ has the smallest ZT with the maximum value of 0.4 at 600C, which was due to the higher thermal conductivity of this structure. Among all compositions, $MnSi_{1.75}$ showed a maximum ZT of 0.55 at 600 °C.

4. Conclusion

In this study, the microstructural and thermoelectric properties of different compositions of nanostructured bulk HMS ($MnSi_x$, $x=1.73$, 1.75 and 1.77) were investigated. It was found that the electrical conductivities of the three samples are similar with that of $MnSi_{1.73}$ nearly 10% larger than the other two compositions. The Seebeck coefficient increased with the increase in the Si content from peak value of ~190 μV/K for $MnSi_{1.73}$ to ~210 μV/K for $MnSi_{1.77}$. Although $MnSi_{1.77}$ has the maximum Seebeck coefficient, the power factor times temperature is approximately equal for all structures. Due to obtaining nanoscale grains, all material compositions showed smaller thermal conductivity than single crystalline HMS, which increased with the increase in the Si content. $MnSi_{1.75}$ showed the smallest thermal conductivity in the range of 2–2.7 W/m K. Overall, nanostructuring did not show significant improvement in ZT compared with that of single crystalline HMS. The different trends in thermal conductivity resulted in the highest value of ZT for $MnSi_{1.75}$, which was 0.55, and the smallest value of ZT for $MnSi_{1.77}$, which was 0.4.

Acknowledgments

The authors thank Liangzhe Li for assisting in instrumentation. This study is partially based upon work supported by the Air Force Office of Scientific Research (AFOSR) High Temperature Materials program under Grant no. FA9550–10–1–0010 and the National Science Foundation (NSF) under Grant no. 0933763.

References

[1] D.M Rowe, Thermoelectrics Handbook: Macro to Nano, CRC press, Boca Raton, FL, 2006.
[2] B. Poudel, Q. Hao, Y. Ma, Y. Lan, A. Minnich, B. Yu, X. Yan, D. Wang, A. Muto, D. Vashaee, X. Chen, J. Liu, M.S. Dresselhaus, G. Chen, Z. Ren, High-thermoelectric performance of nanostructured bismuth antimony telluride bulk alloys, Science 320 (2008) 634–638.
[3] A.J. Minnich, X. Wang, H. Lee, M.S. Dresselhaus, Z.F. Ren, G. Chen, D. Vashaee, Modeling study of thermoelectric SiGe nanocomposites, Physical Review B 80 (2009) 15–21.
[4] S.K. Bux, R.G. Blair, P.K. Gogna, H. Lee, G. Chen, M.S. Dresselhaus, R.B. Kaner, J.P. Fleurial, Nanostructured bulk silicon as an effective thermoelectric material, Advanced Functional Materials 19 (2009) 2445–2452.
[5] D. Vashaee, A. Shakouri, Improved thermoelectric power factor in metallic based superlattices, Physical Review Letter 92 (2004) 106103-1.
[6] J.M. Zide, D.O. Klenov, S. Stemmer, A.C. Gossard, G. Zeng, J.E. Bowers, D. Vashaee, A. Shakouri, Thermoelectric power factor in semiconductors with buried epitaxial semimetallic nanoparticles, Applied Physics Letters 87 (2005) 112102.
[7] M.C. Bost, J.E. Mahan, An optical determination of the bandgap of the most silicon-rich manganese silicide phase, Journal of Electronic Materials 16 (1987) 6–13.
[8] A.J. Zhou, T.J. Zhu, X.B. Zhao, S.H. Yang, T. Dasgupta, C. Stiewe, R. Hassdorf, E. Mueller, Improved thermoelectric performance of higher manganese silicides with Ge additions, Journal of Electronic Materials 39 (2009) 2002.
[9] K. Kakubo, Y. Kimura, Y. Mishima, Microstructures and thermoelectric power of the higher manganese silicide alloys, in: Material Research Society Symposium Proceedings, 646, 2001.
[10] M. Umemoto, Z.G. Liu, R. Omatsuzawa, K. Tsuchiya, Production and characterization of Mn–Si thermoelectric material, Journal of Metastable and Nanocrystalline Materials 8 (2000) 918–923.
[11] S. Zhou, K. Potzger, G. Zhang, A. Mücklich, F. Eichhorn, N. Schell, R. Grötzschel, B. Schmidt, W. Skorupa, M. Helm, J. Fassbender, D. Geiger, Structural and magnetic properties of Mn-implanted Si, Physical Review B 75 (2007) 085203.
[12] I. Kawasumi, M. Sakata, I. Nishida, K. Masumoto, Crystal-growth of manganese silicide, Mn–Si approximately 1.73 and semiconducting properties of Mn15–Si26, Journal of Materials Science 16 (1981) 355.
[13] J.P. Heremans, V. Jovovic, E.S. Toberer, A. Saramat, K. Kurosaki, A. Charoenphakdee, S. Yamanaka, G.J. Snyder, Enhancement of thermoelectric efficiency in pbte by distortion of the electronic density of states, Science 321 (2008) 554–557.

[14] Grob, M. Riffel, U. Stohrer, Journal of Materials Research 10 (1995) 34.
[15] T. Itoh, M. Yamada, Synthesis of thermoelectric manganese silicide by mechanical alloying and pulse discharge sintering, Journal of Electronic Materials 38 (2009) 925–929.
[16] H. Kleinke, New bulk materials for thermoelectric power generation: clathrates and complex antimonides, Chemistry of Materials 22 (2010) 604–611.
[17] S. Xinghua, Z. Zamanipour, A.M. Dehkordi, K.F. Ede, J.S. Krasinski, D. Vashaee, Cost effective synthesis of bulk thermoelectric higher manganese silicide for waste heat recovery and environmental protection, in: Proceedings of IEEE Green Technologies Conference, 2012, pp.1–3.
[18] O.G. Karpinsky, B.A. Evseev, Crystal structure of Mn4–Si7, Izvestiya Akademii Nauk SSSR—Neorganicheskiye Materialy 5 (1969) 525–534.
[19] A.J. Zhou, X.B. Zhao, T.J. Zhu, Y.Q. Cao, C. Stiewe, R. Hassdorf, E. Mueller, Composites of higher manganese silicides and nanostructured secondary phases and their thermoelectric properties, Journal of Electronic Materials 38 (2009) 1072–1077.
[20] V.D. Borman, p.V. Borisyuk, i.V. Tronin, v.N. Tronin, v.I. Troyan, m.A. Pushkin, o.S. Vasiliev, Melting point and lattice parameter shift in supported metal nanoclusters, International Journal of Modern Physics B 23 (2009) 3903–3911.
[21] V.K. Zaitsev, D.M. Rowe (Eds.), CRC Handbook of Thermoelectrics, CRC Press, Boca Raton, FL, 1995 (pp. 299).
[22] M. Umemoto, Z.G. Liu, R. Omatsuzawa, K. Tsuchya, Production and characterization of Mn–Si thermoelectric materia, Materials Science Forum 918 (2000) 343–346.
[23] Takahiro Yamada, Yuzuru Miyazaki, Hisanori Yamane, Preparation of higher manganese silicide (HMS) bulk and Fe-containing HMS bulk using a Na–Si melt and their thermoelectrical properties, Thin Solid Films 519 (2011) 8524–8527.
[24] Y.J. He, Q.R. Hou, Z.M. Wang, Y.B. Chen, Thermoelectric properties of MnSi1.7, in: IEEE International Conference on Materials for Renewable Energy and Environment (ICMREE), 2, 2011, pp. 1343–1345.
[25] D.B. Migas, V.L. Shaposhnikov, A.B. Filonov, V.E. Borisenko, N.N. Dorozhkin, Ab initio study of the band structures of different phases of higher manganese silicides, Physical Review B 77 (2008) 0752051–0752059.